Progress In Electromagnetics Research M, Vol. 31, 1–11, 2013

TERRAIN HEIGHT ESTIMATION USING A STEREO-SAR TECHNIQUE AIDED BY A REFERENCE POINT

Kung-Yu Lu[1, 2] and Jean-Fu Kiang[1, 2, *]

[1]Department of Electrical Engineering, National Taiwan University, Taipei, Taiwan

[2]Graduate Institute of Communication Engineering, National Taiwan University, Taipei, Taiwan

Abstract—A stereo-synthetic aperture radar (stereo-SAR) technique is proposed to estimate the terrain height of a target area. A reference point with known altitude is located within the target area to calibrate the height estimation. The estimated height error can be reduced to one meter. This method requires the processing techniques of conventional SAR, while achieving a fairly fine resolution in height estimation for practical applications.

1. INTRODUCTION

Airborne or satellite-borne synthetic aperture radars (SAR's) have been widely used to acquire high-resolution images of remote terrains or ocean surfaces [1–3]. Stereo techniques based on optical images have been used to estimate terrain profiles, usually accompanied by a digital elevation model (DEM) or a digital terrain model (DTM). Ground control points (GCP's) are usually adopted in the stereo techniques to improve the accuracy of height estimation. In [4], on-board satellite data are used to derive a pair of SPOT stereo-strips for three-dimensional positioning. Experimental results indicate that, on a SPOT panchromatic stereo-strip of 45 km × 280 km, the root-mean-square-error is less than 8 m in each direction when four GCP's are used.

In [5], a least-square collocation method is applied to a rational function model (RFM) to compensate for local system errors. The rms

Received 19 March 2013, Accepted 8 May 2013, Scheduled 15 May 2013

* Corresponding author: Jean-Fu Kiang (jfkiang@cc.ee.ntu.edu.tw).

error is 1.91 m when using the images from SPOT 5, plus 9 GCP's; and is 0.6 m when using the images from QuickBird, plus 9 GCP's.

In [6], a batch iterative least-squares (BILS) and an incremental discrete Kalman filtering (IDKF) methods are proposed. With 20 additional GCP's, the rms height error is reduced from 3.383 to 2.42 and 2.282 m. In [7], a few GCP's are used to determine the boresight alignment angles, in order to correct the orientation of the images and to improve the accuracy of the digital surface model (DSM) and orthoimage. Using 3–4 GCP's to estimate the boresight alignment angles related to the stereo data of the high-resolution stereo (HRS) images on SPOT 5, it is possible to reach a co-registration accuracy of less than 3 m, as well as to reduce the height bias in the Catalonian case from 9 to 2 m.

In [8], a sensor model, including system error, is proposed to retrieve correct satellite orbit and attitude angle. The parameters of this correction model can be further improved if a small number of GCP's are available. From the images over Melbourne and Bhutan areas taken by three satellites, QuickBird, SPOT 5 and ALOS PRISM, respectively; the offset due to orbit and attitude uncertainties can be narrowed down to one pixel. In [9], a rational polynomial coefficient block adjustment model is proposed for image processing. The average height error is 1.6 m if no GCP's are used, and is reduced to 0.2 m if some GCP's are available.

In [10], a three-dimensional radar-grammetric model is applied to high-resolution RADARSAT-2 images. The localization and restitution error is 1 m in the horizontal plane and 2 m in height. The average height error and standard deviation embedded in these data are 4.4 m and 6.3 m, respectively. In [11], an elevation error model is applied to the high-resolution DEM's developed from stereo-image processing, and the resulting rms error of height varies between 1.67 and 2.9 m.

In [12], a DEM is generated over a mid-slope region in Abukuma Highland, Fukushima Prefecture, Japan, based on the JERS-1 stereoscopic data. Without using any GCP's, the rms error of height is 57 m. In [13], a multi-image matching technique is applied to generate a digital surface model, based on a geometrically constrained matching. By comparing with the lidar data, the rms height error over forests turns out to be less than 2 m.

Interferometric SAR (InSAR) and polarimetric InSAR (PolInSAR) have been widely used to reconstruct terrain profiles. The latter is more often used for terrains covered with vegetation or trees. In [14], the tree-stand heights are retrieved using the height and ancillary data of the C-band Shuttle Radar Topography Mission (SRTM). The rms error is 2.5–3.6 m, much better than the 6.8–8.3 m retrieved

from the raw SRTM-National Elevation Dataset (SRTM-NED). In [15], the height profile is estimated using the X-band PolInSAR data of an airborne system, Radar Aeroporte Multi-spectral d'Etude des Signatures (RAMSES). Typical vegetation height is around 30 cm, smaller than the height accuracy of the data. The building height over urban areas can also be estimated to reach 1 m of accuracy.

A three-stage inversion process is applied to PolInSAR data of tress in the L-band, collected with an electronically scanned array (ESA) [16], and the rms error of height is 3.547 m. Airborne laser scanning (ALS) data have also been used to monitor forest height profiles [17], with an rms height error of 2.3 m.

In this work, a stereo-SAR technique is proposed to reconstruct the terrain profiles, with one reference point or ground control point in the target area. This technique is less sophisticated than the InSAR techniques, yet its accuracy is fair for some practical applications. The proposed technique is presented in Section 2, simulations and analysis over three different types of terrain are presented in Section 3, and the conclusion is drawn in Section 4.

2. STEREO-SAR TECHNIQUE

2.1. Review of SAR Technique

Figure 1 shows the flow-chart of the range-Doppler SAR algorithm used in this work. To conduct range compression, the received data are Fourier transformed in the range domain using the FFT, multiplied by a range-match filter, then inverse transformed using the IFFT. Similarly, the azimuth compression is conducted by Fourier transforming the processed data in the Doppler domain, aligning the output at the same range using an RCMC algorithm, applying an azimuth-match filter, then inverse transforming the results to obtain the final image data.

2.2. Processing Algorithm

Figure 2(a) shows two flight paths, S_1 and S_2, with the same altitude h, of two satellites in one pass or one satellite in two passes. The along-track separation is zero, and the across-track separation is r_d. The position of satellite(s) can be recorded to an accuracy level of cm using the DGPS technique recently reported in [18].

Figure 2(b) shows the schematic to estimate the terrain profile of the target area using one reference object with known height. The target area is divided into rectangular cells of size Δx and Δy in the x and y direction, respectively. Consider the target object, P_t, at the

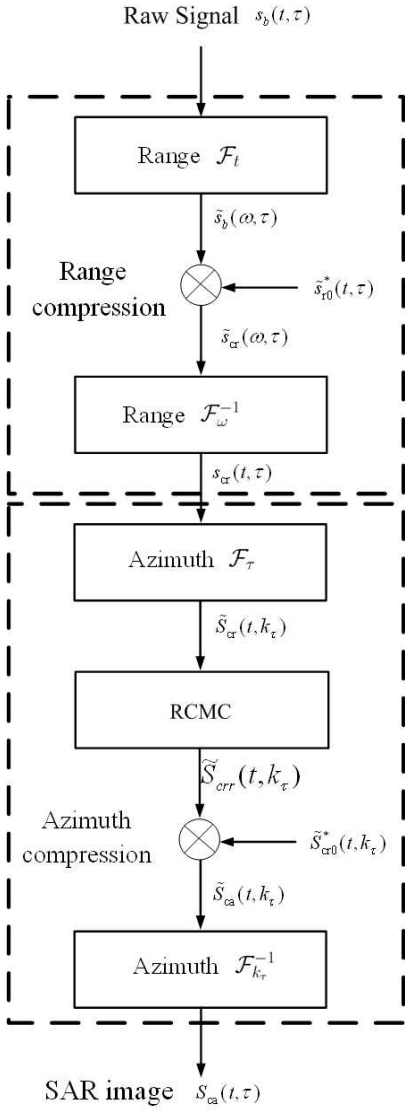

Figure 1. Flow-chart of range-Doppler SAR.

horizontal location $((n+1)\Delta x, y)$, with an unknown height of z; the reference object is located at $(n\Delta x, y)$, with a known height of z_r. The distances from P_t to S_1 and S_2 are R_1 and R_2, respectively, θ_1 is the

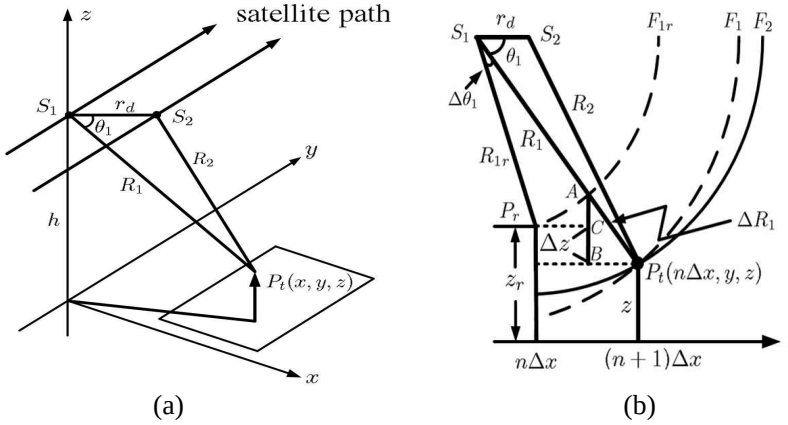

Figure 2. (a) Configuration of dual satellite paths over a target area. (b) Estimation of θ_1 using R_1, R_2 and r_d; height estimation using ΔR_1 and θ_1.

angle between $\overline{S_1P_t}$ and $\overline{S_1S_2}$. By the cosine law,

$$\theta_1 = \cos^{-1} \frac{R_1^2 + r_d^2 - R_2^2}{2R_1 r_d} \tag{1}$$

In practice, $\Delta x, z, z_r \ll R_{1r}, R_1$, and $\theta_1 > 30^\circ$. If $z \leq z_r$, it is observed that $R_{1r}\Delta\theta_1 \leq R_1\Delta\theta_1 \simeq \Delta x/\sin\theta_1$, which implies that $\Delta\theta_1 \leq \Delta x/(R_{1r}\sin\theta_1) \simeq 0$. If $z_r < z$, it is observed that $R_1\Delta\theta_1 \simeq \Delta x/\sin\theta_1 + (z - z_r - \Delta x\cot\theta_1)\cos\theta_1$, which implies $\Delta\theta_1 \simeq 0$. Either way, the angle $\Delta\theta_1$ can be approximated as zero.

The ranges $R_1 = |\overline{S_1P_t}|$ and $R_{1r} = |\overline{S_1P_r}|$ can be estimated from the SAR image data retrieved from satellite 1 or pass 1, and $\Delta R_1 = |\overline{AP_t}| = R_1 - R_{1r}$. The height difference is estimated as $\Delta z = z_r - z = |\overline{BC}| \simeq |\overline{AB}| = \Delta R_1 \sin\theta_1$ if $z \leq z_r$, hence the target height can be estimated as $z = z_r - \Delta R_1 \sin\theta_1$. Similarly, when $z_r < z$, the target height can be estimated as $z = z_r - \Delta R_1 \sin\theta_1$, where ΔR_1 is less than zero.

Given the coordinates and height of the reference object, the distances $R_{1r} = |\overline{S_1P_r}|$ and $R_{2r} = |\overline{S_2P_r}|$ can be calculated *a priori*. By applying the conventional SAR processing techniques, as shown in Figure 1, to the data received over flight path S_1, the echo times to S_1 from the target and the reference objects are estimated as t_1 and t_1', respectively. Similarly, by processing the data received over path S_2, the echo times to S_2 from the target and the reference objects are estimated as t_2 and t_2', respectively. The distance R_1 is calculated as

$R_1 = R_{1r} + c\Delta t_1/2$, where c is the speed of light and $\Delta t_1 = t_1 - t_1'$. Similarly, R_2 is calculated as $R_2 = R_{2r} + c\Delta t_2/2$, with $\Delta t_2 = t_2 - t_2'$. The echo times t_1, t_2, t_1' and t_2' are retrieved directly from the relevant SAR image data, no phase synchronization between S_1 and S_2 is required.

The height of target object at $((n-1)\Delta x, y)$ is estimated in a similar manner. Once the heights of target objects at $((n+1)\Delta x, y)$ and $((n-1)\Delta x, y)$ are estimated, they can be used as the reference height to estimate the heights at $((n+2)\Delta x, y)$ and $((n-2)\Delta x, y)$, respectively. By induction, this process can be continued to estimate the heights of the target objects in the same row at a given y.

3. SIMULATIONS AND DATA ANALYSIS

Table 1 lists relevant parameters of the TerraSAR-X satellite used in our simulations [19]. Assume the target area is centered at $(x_c, y_c) = (350, 0)$ km, and is divided into square cells of size $\Delta x \times \Delta y$. A total of 8192 pulses are emitted along the track, and the pulse repetition interval is chosen to be $\Delta\tau = 43.86\,\mu$s, making an effective aperture length of $L = 8192V\Delta\tau = 2560$ m.

Table 1. Parameters of TerraSAR-X satellite.

Parameter	Symol	Value
Altitude of satellite	h	750 km
Carrier frequency	f_0	9.65 GHz
Bandwidth	B_w	150 MHz
Time resolution	Δt	1.25 ns
Chirp pulse duration	T_p	25 µs
Satellite ground speed	V	7125 m/s
Chirp rate	K_r	6 THz/s

Figure 3 shows the response of a point-like target object using the SAR processing algorithms. The 3 dB ground resolutions in the range and the azimuth directions are 5 m and 7 m, respectively. Hence, the postspacings of the target areas are chosen to be $\Delta x = 30$ m and $\Delta y = 30$ m. Theoretically, the range resolution is on the order of $\Delta R = c/(2B_w) \simeq 2$ m, and the azimuth resolution is on the order of $\Delta R_a = \lambda R/(2L) \simeq 5$ m.

Figure 4 depicts three target areas chosen for simulation:

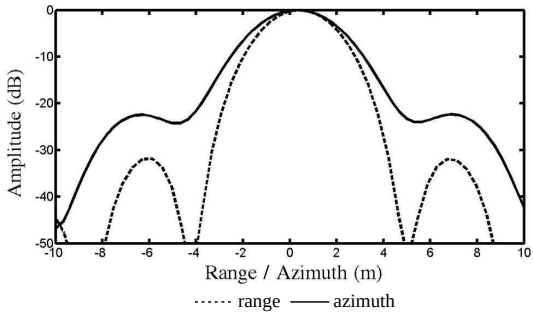

Figure 3. Response of a point-like scatterer.

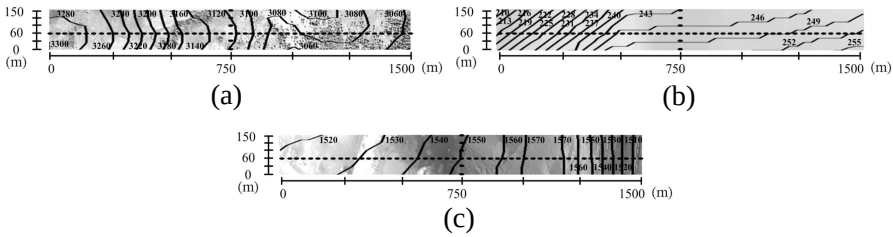

Figure 4. Contour map and image of (a) Nanshuangtou Mountain in Zhuoxi Township, Hualien County, Taiwan, (b) glacier in the west Antarctic, (c) Eyjafjallajokull Volcano in southern Iceland.

The Nanshuangtou Mountain in Zhuoxi Township, Hualien County, Taiwan; Glacier in the west Antarctic; and Eyjafjallajokull volcano in southern Iceland [20]. The SAR images of these target areas are simulated using the height profiles retrieved from the Google Earth.

3.1. Nanshuangtou Mountain in Zhuoxi Township, Hualien County, Taiwan

Flight safety over eastern Taiwan has been a serious issue aroused by several aircraft crashes. In the morning of August 30, 2012, an aircraft of the ROC Aviation Company fell, due to bad weather and complicated terrain profile, in Nanshuangtou mountains in Zhuoxi Township, Hualien County, claimed the lives of three crew members.

Figure 4(a) shows a strip area in the subject region, with the terrain height ranging from 3038 to 3300 m. Figure 5(a) shows the estimated height error. The rms error is $e_r = 1.4447$ m if the third row of data as marked in Figure 4(a) are used, and is $e_r = 1.455$ m if all six rows of data are included.

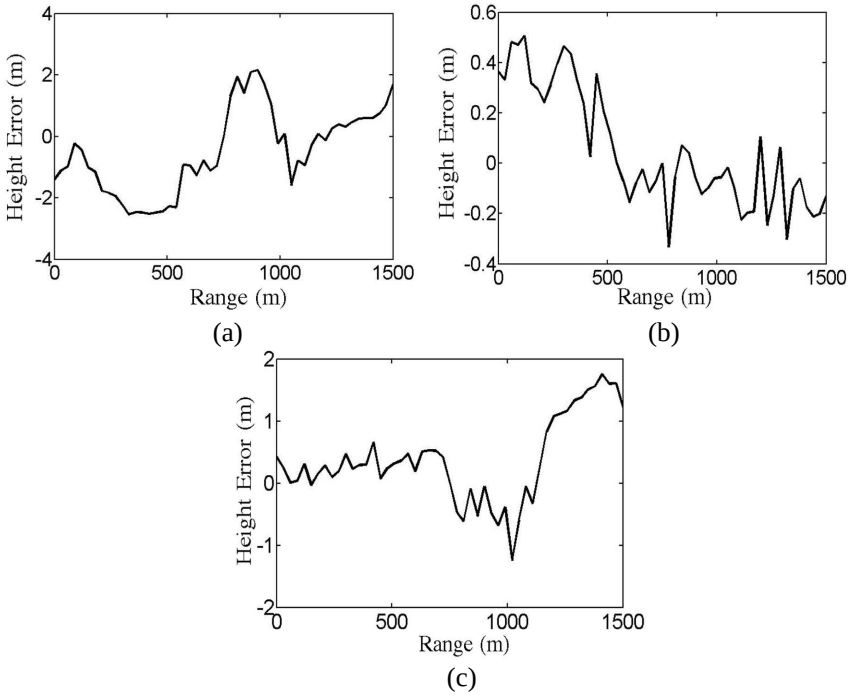

Figure 5. Height error along the center row of the strip area in (a) Nanshuangtou Mountain in Zhuoxi Township, Hualien County, Taiwan, (b) glacier in the west Antarctic, (c) Eyjafjallajokull Volcano in southern Iceland.

3.2. Glacier in the West Antarctic

Breakdown of ice sheet in the west Antarctic has been reported in the February 6, 2009 issue of *Science* magazine [21], including the largest Ross Ice Shelf and Ronne Ice Shelf. Figure 4(b) shows a strip area in the west Antarctic, with the terrain height ranging from 207 to 256 m. Figure 5(b) shows the estimated height error. The rms error is $e_r = 0.2378$ m if the third row of data as marked in Figure 4(b) are used, and is $e_r = 3.5897$ m if all six rows of data are included.

3.3. Eyjafjallajokull Volcano in Southern Iceland

The Eyjafjallajokull volcano in southern Iceland erupted on April 14, 2007 and March 20, 2010, separately, gushing a large amount of ashes. Many European airports were shut down, causing the airline industry to lose 200 million dollars a day, not to mention the rippling

effects upon other industries. Figure 4(c) shows a strip area in the subject region, with the terrain height ranging from 1503 to 1577 m. Figure 5(c) shows the estimated height error. The rms error is $e_r = 0.758$ m if the third row of data as marked in Figure 4(c) are used, and is $e_r = 1.4463$ m if all six rows of data are included.

3.4. Discussions

The proposed stereo-SAR technique can be used to monitor the change of terrain profiles, for example, landslides, ice caps, among many others. Landslides take place in many areas of the world, including Taiwan. Some landslides may create landslide dam in deep forests or valleys, without being noticed, and the residents living in the downstream may suffer from its breakdown later. With the fast development of satellite constellation for remote sensing, this technique can become feasible and practical to constantly monitor vast areas.

In this technique, only one reference point or ground control point is required, but no DTM or DEM is demanded. Since the LEO satellites fly hundreds of km above the target area, height estimation based on phase detection, as in the InSAR technique, is quite sophisticated. This technique is based on the echoed time of signal instead of the phase, hence is relatively easier to implement.

4. CONCLUSION

A stereo-synthetic aperture radar (stereo-SAR) technique is proposed to reconstruct the height profile of terrains, requiring only one reference point. The technical parameters of TerraSAR-X satellite are chosen to simulate over three different types of terrain. The rms error of height estimation can be reduced to one meter, making this technique practical for certain applications.

ACKNOWLEDGMENT

This work was sponsored by the National Science Council, Taiwan, ROC, under contract NSC 99-2221-E-002-055.

REFERENCES

1. Stimson, G. W., *Introduction to Airborne Radar*, 2nd edition, SciTech, 1998.
2. Soumekh, M., *Synthetic Aperture Radar Signal Processing with MATLAB Algorithms*, Wiley-Interscience, 1999.

3. Cumming, I. G. and F. H. Wong, *Digital Processing of Synthetic Aperture Radar Data Algorithms and Implementation*, Artech House, 2005.
4. Chen, L.-C. and L.-Y. Chang, "Three-dimensional positioning using SPOT stereo strips with sparse control," *J. Surveying Eng.*, Vol. 124, No. 2, 63–72, May 1998.
5. Chen, L.-C., T.-A. Teo, and C.-L. Liu, "The geometrical comparisons of RSM and RFM for FORMOSAT-2 satellite images," *Photogram. Eng. Remote Sens.*, Vol. 72, No. 5, 573–579, May 2006.
6. Hu, Y. and C.-V. Tao, "Updating solutions of the rational function model using additional control information," *Photogram. Eng. Remote Sens.*, Vol. 68, No. 7, 715–723, Jul. 2002.
7. Reinartz, P., R. Muller, M. Lehner, and M. Schroeder, "Accuracy analysis for DSM and orthoimages derived from SPOT HRS stereo data using direct georeferencing," *ISPRS J. Photogram. Remote Sens.*, Vol. 60, 160–169, Jul. 2006.
8. Weser, T., F. Rottensteiner, J. Willneff, J. Poon, and C. S. Fraser, "Development and testing of a generic sensor model for pushbroom satellite imagery," *Photogram. Eng. Remote Sens.*, Vol. 71, No. 11, 1321–1327, Nov. 2005.
9. Grodecki, J. and G. Dial, "Block adjustment of high-resolution satellite-images described by rational polynomials," *Photogram. Eng. Remote Sens.*, Vol. 69, No. 1, 59–68, Jan. 2003.
10. Toutin, T. and R. Chenier, "3-D radargrammetric modeling of RADARSAT-2 ultrafine mode: Preliminary results of the geometric calibration," *IEEE Trans. Geosci. Remote Sens. Lett.*, Vol. 6, No. 3, 611–615, Jul. 2009.
11. Davis, C. H., H. Jiang, and X. Wang, "Modeling and estimation of the spatial variation of elevation error in high resolution DEMs from stereo-image processing," *IEEE Trans. Geosci. Remote Sens.*, Vol. 39, No. 11, 2483–2489, Nov. 2001.
12. Miyazaki, Y., T. Osani, and H. Watanabe, "Digital terrain model of JERS-1 data for ASTER VNIR stereo application," *IEEE Int. Geosci. Remote Sens. Symp.*, Vol. 1, 131–133, Aug. 1993.
13. Kenyi, L. W., R. Dubayah, M. Hofton, and M. Schardt, "Comparative analysis of SRTMVNED vegetation canopy height to LIDAR-derived vegetation canopy metrics," *Int. J. Remote Sens.*, Vol. 30, No. 11, 2797–2811, Jun. 2009.
14. Brown, C. G., K. Sarabandi, and L. E. Pierce, "Model-based estimation of forest canopy height in red and Austrian pine

stands using shuttle radar topography mission and ancillary data: A proof-of-concept study," *IEEE Trans. Geosci. Remote Sens.*, Vol. 48, No. 3, 1105–1118, Mar. 2010.

15. Garestier, F., P. D. Fernandez, X. Dupuis, P. Paillou, and I. Hajnsek, "PolInSAR analysis of X-band data over vegetated and urban areas," *IEEE Trans. Geosci. Remote Sens.*, Vol. 44, No. 2, 356–364, Feb. 2006.
16. Tan, L. and R. Yang, "Investigation on tree height retrieval with polarimetric SAR interferometry," *IEEE Int. Geosci. Remote Sens. Symp.*, 546–549, Jul. 2008.
17. Solberg, S., D. J. Weydahl, and E. Masset, "Simulating X-band interferometric height in a spruce forest from airborne laser scanning," *IEEE Trans. Geosci. Remote Sens.*, Vol. 48, No. 9, 3369–3378, Sep. 2010.
18. Tsai, S.-C. and J.-F. Kiang, "Floating dropsondes with DGPS receiver for real-time typhoon monitoring," *IEEE Trans. Geosci. Remote Sens.*, Vol. 49, No. 11, 4363–4373, Nov. 2011.
19. Buckreuss, S., R. Werninghaus, and W. Pitz, "German satellite mission TerraSAR-X," *IEEE Aero. Electron. Syst. Mag.*, Vol. 24, No. 11, 4–9, Nov. 2009.
20. Google Earth Software for Microsoft Windows, Ver 6.2.
21. Online, http://www.anntw.com/awakening/news_center/show.php?itemid=37489.